Hessian-based neck tracing of dendritic spines: a preliminary study on confocal images

E. Bruno[1], S. Cauzzo[2], A. L. Callara[1,2], A. Ahluwalia[1,2], C. Magliaro[2] and N. Vanello[1,2]
[1] *Dipartimento di Ingegneria dell'Informazione, University of Pisa, Pisa, Italy*
[2] *Research Center "E. Piaggio", University of Pisa, Pisa, Italy*

***Abstract*— Alterations in dendritic spines morphology and topology are known to be implied in several neurodegenerative diseases. However, visualizing and reconstructing the exact morphology of spine necks using conventional confocal imaging is still a challenge. In the light of this, we propose the extension of Hessian matrix eigenvalue analysis for the detection of tubular structures to the problem of 3D neck tracing. In this work we stress the relevance of the tracing procedure initialization, for the novel application of this standard approach to the specific scenario. Preliminary results on confocal microscopy images from ex-vivo human samples allowed to obtain almost 80% of necks keeping an average distance of less than one voxel from the reference segmentation and half of them fully overlapping with it. The preliminary results are promising, since they pave the way towards the development of this model-free solution to accurately trace spine neck.**

***Keywords*—Confocal microscopy, pyramidal cells, dendritic spines, tracing, neuronal reconstruction.**

I. Introduction

Dendritic spines are neuronal protrusions implied in synaptic function, supporting learning, memory and motivation [1]–[6]. Changes in spine density, size, shape and distribution have been detected in neurodegenerative diseases such as Alzheimer's, autism spectrum disorders and many others [7]–[9]. To this end, quantitatively characterizing such features would be of particular interest. However, obtaining faithful information on dendritic spine morphology is not an easy task. Indeed, spines necks have a thin and small structure which is hard to discriminate with conventional microscopy, since its size is close to the optical resolution limit of the imaging techniques [10]. On the other hand, the high density of spines makes the manual or a semi-automatic segmentation tedious and time-consuming, increasing the necessary introduction of automatic procedures.

Several approaches have been proposed for reconstructing spine necks. Some of them require a large database of images to create a library of deformable models [11] or train convolutional neural networks [12]. Models based on global approaches to segmentation might fail in detecting spine necks given the different signal-to-noise ratio (SNR) properties of small structures [13], [14]. Thus, approaches based on local intensity or morphological local characteristics were proposed [14]–[18]. One of the most adopted tools, NeuronStudio [16] exploits local geometrical models. However, this approach is optimized for head spine detection and is suboptimal for neck spine shape characterization. In [17], a curve based on Legendre functions is fitted between dendrite shafts and detached spine head in 2D microscopy images, to adapt to different possible neck geometries. Geometrical features, as those based on tubular structures exploited in [19] for vascular tree, was evaluated in [18]. Specifically, eigenvalue analysis of the Hessian matrix has been introduced to define vesselness measures in biomedical images [19]. In fact, within tubular structures, the smallest-magnitude eigenvalue of Hessian is associated with the eigenvector directed along the minimum intensity variation, i.e., the longitudinal axis of the tubular structure. In [18] the information from local Hessian matrix was used to design an adaptive filter for dendrite tracing and spine head detection. The approach proved to achieve a good performance on stimulated depletion image but was not applied to image stacks.

In this work, we present a novel neck-tracing approach that exploits the eigenvalue analysis of the Hessian matrix. Specifically, the proposed method will be applied to images where both dendrites and spine heads have already been segmented. The aim is to correctly identify and trace the spine necks. We will point out the relevance of the tracing algorithm initialization and we will propose and evaluate different strategies. We test our method on 3D stacks of confocal images of a human pyramidal cell dendrite. We validate our approach against ground truth assisted segmentation of spines performed by expert-users.

II. Material and Methods

A. Experimental data

We processed a confocal image stack of an intracellular injected layer III pyramidal neuron from the human brain cingulate cortex (freely available for the scientific community and presented in [20]). Sections were imaged with a Leica TCS 4D confocal scanning laser equipped with to a Leitz DMIRB fluorescence microscope. All the data was also provided with a reference segmentation of the dendritic branch and spines reconstructed manually using Imaris 6.4.0 (Bitplane AG, Zurich, Switzerland).

B. Neck tracing procedure

Tracing a neck consists in connecting two disconnected clusters of segmented voxels, one linked to the spine head, and one linked to the dendrite. Therefore, to test our approach, we firstly performed a binary segmentation of the intensity image leaving some spines disconnected. We created such segmentation employing Otsu's method in the Icy software [21] which defines the optimal threshold based on the observed intensity distribution of pixel values. We refer to this segmentation as Otsu segmentation, OS [22]. The proper neck tracing approach is run on the unsegmented portions of the intensity image, and it is composed of an initialization phase

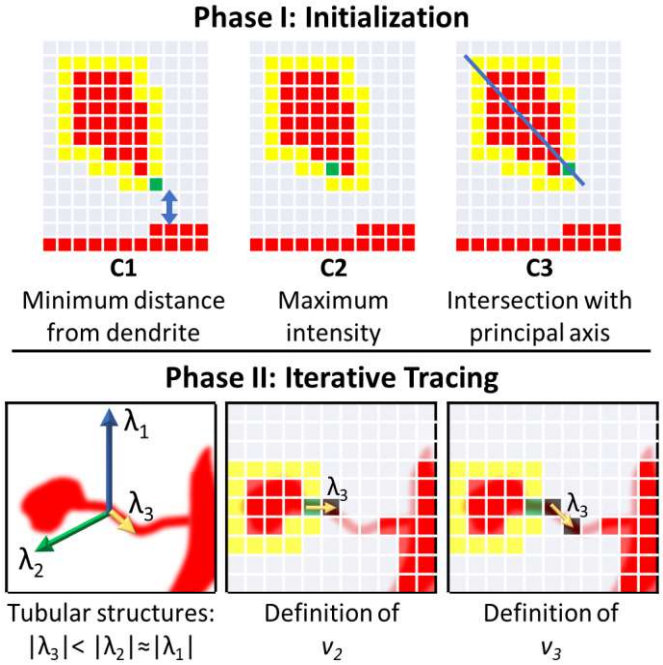

Fig. 1 Schematization of the neck tracing approach. OS is marked in red, OB in yellow. Phase I) selection of the first voxel in the trace among those in OB, with the three tested criteria. Phase II) thanks to the properties of the Hessian matrix eigenvalues within tubular structures, the neck can be traced by 1) performing the eigenvalue analysis at voxel v_i; 2) defining v_{i+1} as the neighboring voxel intersected by the smallest eigenvector.

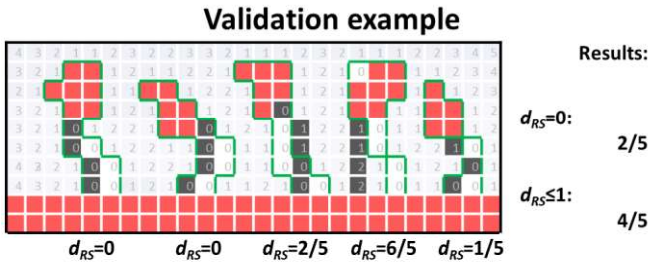

Fig. 2 Validation example simplified in a 2D case: necks (black) connecting disconnected clusters of OS (red) are compared against RS (white with green borders) in terms of average Euclidian distances. Distance values in cells are rounded to the highest integer.

(phase I) aiming at selecting the starting seed of the path-finding phase (phase II). The approach is sketched in Fig. 1.

Phase I defines the first voxel of the trace among those composing the outer border (OB) of the disconnected spine. We tested 3 different criteria: C1) the voxel in OB that is closest to the dendrite in terms of Euclidean distance; C2) the maximum intensity voxel within OB; C3) the voxel in OB intersected by the principal axis of the spine, placed on the side of OB that is closest to the dendrite.

Instead, phase II consists of a one-voxel step procedure starting from the first voxel and iteratively repeated to define the trace of the neck. For each voxel v_i in the trace, the Hessian matrix is defined computing the second order derivatives D_{xx}, D_{yy}, D_{zz}, D_{xy}, D_{xz}, D_{yz}. Eigenvectors and eigenvalues of the Hessian matrix are then extracted. Eigenvalues encode the information on second-order intensity variability along the axis defined by the eigenvector. Within a tubular structure, the direction parallel to the main axis is the one meeting no structure boundaries, i.e., the one along which the smallest intensity variations occur. This situation, schematized in the lower-left panel of Fig. 1, can be summarized by the formula $|\lambda_3| < |\lambda_2| \approx |\lambda_1|$. Therefore, starting from v_1 as defined in Phase I (shown in green in Fig. 1), v_2 is chosen within the 26-neighborhood of v_2 as the voxel being intersected by the eigenvector of the Hessian matrix associated to the smallest absolute eigenvalue λ_3, visualized with a golden arrow in Fig. 1. The procedure is repeated starting from v_2 to define v_3 (lower-right panel in Fig. 1), and then iterated on each v_i, to define v_{i+1}, until the trace meets the dendrite, or a given number of steps, Max_Steps, is reached. Max_Steps is identified to avoid the algorithm getting lost in a non-tubular structure or failing to reach the dendrite.

C. Validation

We preliminary validated our method on 350 spines included in one image stack. A gold-standard semi-automatic segmentation of these spines was published in [20] and is here labelled as Reference Segmentation, RS. This ground-truth was obtained with the software Imaris by combining spine-by-spine segmentations defining multiple ad hoc binary thresholds. Among the total number of spines, we focused only on those disconnected (26-neighbors) from the dendrite in the OS.

The tracings obtained using the three initialization strategies were evaluated, using a distance measure d_{RS} of each traced neck from the RS. Such measure is 0 when all the voxels in the neck overlap with the reference segmentation, and non-zero otherwise. The validation measure d_{RS} was estimated as it follows:

- For each voxel of the traced neck
  - we assign 0 if the voxel belongs to the RS
  - we estimate the Euclidean distance d_{RS} from the edge of the RS
- We average the obtained value across the voxels of the considered neck, to obtain the average d_{RS}

Using this approach, we can provide a quality assessment also for necks that do not fully overlap with RS.

III. Results

A. Quantitative analysis

Out of the 350 spines marked in RS, OS results in 88 spines disconnected from the structure core. We observed that segmented spines are separated on average by less than 10 voxels from the segmented dendrite, so we empirically set Max_Steps to 20. In Fig. 3, we report the quantitative evaluation of the three initialization criteria implemented for phase I, in terms of percentage of necks that fully overlap with RS, i.e., that show $d_{RS} = 0$, and percentage of necks showing $d_{RS} \leq 1$. C2 is the criterion providing the best results, with $d_{RS} = 0$ for the 47.7% of the 88 necks and $d_{RS} \leq 1$ for the 77.3% of them.

B. Neck reconstructions

In Fig. 4, we report four examples of traced necks, visualized with 3D reconstructions and overlayed on OS and RS. We observe that, with a good approximation, the majority

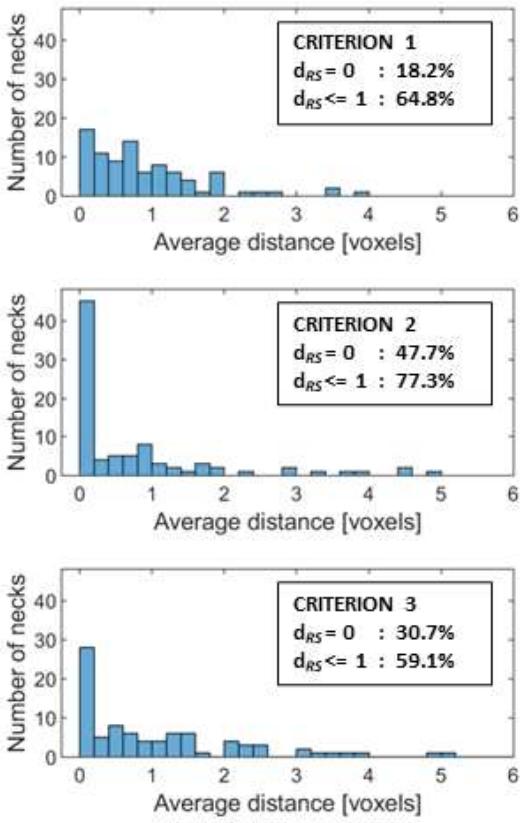

Fig. 3 Evaluation of the three initialization approaches of phase I in terms of average distance from RS for the 88 disconnected spines.

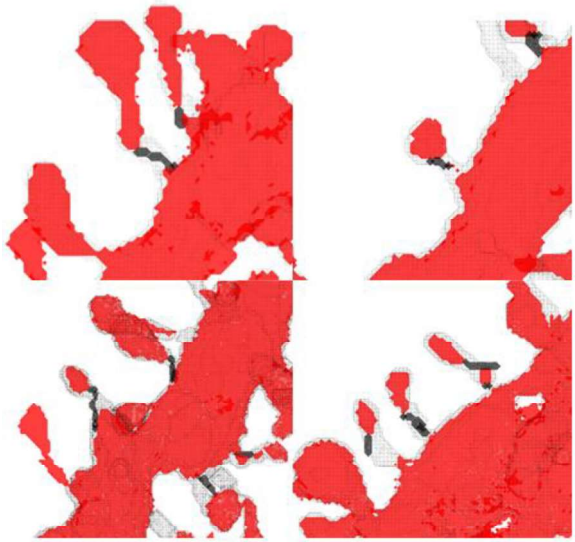

Fig. 4 Four examples of necks reconstructed by the algorithm (in black) overlaying OS (red) RS (gray).

spines have been successfully connected with the proper section of the dendrite.

IV. Discussions

In this work, we present a novel approach for spine neck reconstruction using the local information of the Hessian matrix. The geometrical information achievable by such analysis was already exploited for spatial filter design in [19] for spine head and neuron tracing. To our knowledge, the implementation for spine neck sequential tracing presented here is novel. Moreover, by testing three initialization criteria, we highlighted the relevance of this phase and assessed the maximum intensity voxel within the outer border of the spine as best starting point. With this criterion, we obtain a good percentage of tracings being in line with a published reference segmentation produced with a deep learning-based approach.

For the image used in this work, a reference segmentation RS capable of keeping spines connected to the corresponding dendrite was already available, since spine and neck identification was obtained using a manual 3D reconstruction of the same image sample performed with the software Imaris. Future tests will be required on samples on which a segmentation able to keep spines connected has not yet been achieved. This could be the case of confocal standard- or super-resolution STED images from clarified tissue. These tests will require a validation based on manual segmentation and a comparison against other available methods.

Due to the image type, which describes injected cells, and due to the bimodality of the intensity histogram, Otsu's method, that exploits a global intensity threshold, was selected as one of the simple strategies to segment this type of dataset. However, other methods employing different segmentation strategies can be used [23] and their results merged with the proposed approach when spine neck segmentation is failing.

To validate our results, we designed a strategy that estimates an average distance of the reconstructed neck from the RS. Since RS can be as thin as a single voxel, this strategy better characterizes the results with respect to a binary decision on a complete overlap between the reconstruction and the RS. We provide histograms of the average Euclidean distances between necks and RS, and we report the percentage of necks showing $d_{RS} \leq 1$, considered as satisfying reconstructions. In this work, this validation measure is also used to compare the three initialization criteria, highlighting a far better performance by C2 with respect to both C1 and C3 (Fig.3). Performance of the minimum distance criterion (C1) is impaired by the neck curvatures, which are often bent with respect to the direction normal to the dendrite surface. The performance of spine principal axis criterion (C3) is impaired by the multiple shapes that can be assumed by spine heads [24], which can present very wide caps and thus a principal axis that is aligned to the dendrite. Choosing the highest-intensity sub-threshold voxel resulted to be the best initialization criterion. In addition, on segmentations that do not rely on the sole magnitude (e.g., segmentation algorithms based on deep learning [11], [25], [26] structure enhancement filters [27], [28] or statistical modelling [29]), the use of C3 might not be optimal and should be further tested.

We have to stress that the generalizability of C2 criterion to images with lower SNR, with respect to the one here analysed, should be further tested. In fact, this solutionis likely to be sensitive to noise since it selects the maximum intensity voxel. As a result, a different criterion could better perform on a different image type.

We observed that definitions of the starting point on the wrong side of the spine produce erroneous tracings that could hardly be recovered. In this light, further research on the proper initialization of neck tracing algorithms is crucial. Future developments should focus on providing a less local definition of maximum intensity, e.g., adopting smoothing

filters in phase I prior to applying C2, or employing measures based on percentiles within a neighbourhood. Similarly, in phase II the eigenvalue analysis could be conducted with an approach that is still local, but less punctual, to be more robust to noise. A more noise-robust local eigenvalue analysis should impact the performance as well in Phase II: this could be achieved in the computation of the Hessian by weighing the contribution of a neighbourhood of voxels, e.g. using convolutions with derivatives of gaussians instead of punctual differentiation, as in [19], [30].

As our algorithm does not perform spine assignment, the presence of spines belonging to different dendrites within the same stack could lead it to the tracing of non-existing necks. To target this issue, in an interesting future development a crucial preliminary spine assignment step based on a 3D watershed transform could be integrated in the algorithm.

An application of our approach on super-resolution techniques (e.g., STED, STORM), which allow to resolve spine morphology even in clarified thick slices (500 μm), will be also explored in the future.

V. Conclusion

We present an algorithm to detect neck spines using an approach based on the Hessian matrix eigenvalue analysis applied to confocal microscopy. The centrality of initialization is addressed, assessing important changes in algorithm performance when different initialization criteria are employed. Our results suggest that a precise tracking of spine necks could be obtained using a model-free solution. An accurate reconstruction of spine necks will help to define the morphology of the synaptic transmission centre implied in neurodegenerative diseases.

Acknowledgement

The authors deeply thank the group of Professor Javier De Felipe at the Universidad Politécnica de Madrid for sharing data. This work was supported by the FLAG-ERA JTC 2019 project SENSEI (Partnering Project of the Human Brain Project, CUP: I54I19002660006). Research partly funded by the European Union - Next Generation EU, in the context of The National Recovery and Resilience Plan, Investment 1.5 Ecosystems of Innovation, Project Tuscany Health Ecosystem (THE), Spoke 3 "Advanced technologies, methods, materials and heath analytics " CUP: I53C22000780001.

References

[1] R. Yuste, A. Majewska, and K. Holthoff, “From form to function: calcium compartmentalization in dendritic spines,” *Nat. Neurosci.*, vol. 3, no. 7, pp. 653–659, 2000

[2] K. M. Harris and S. B. Kater, “Dendritic Spines: Cellular Specializations Imparting Both Stability and Flexibility to Synaptic Function,” *Annu. Rev. Neurosci.*, vol. 17, no. 1, pp. 341–371, 1994

[3] J. Bourne and K. M. Harris, “Do thin spines learn to be mushroom spines that remember?,” *Curr. Opin. Neurobiol.*, vol. 17, no. 3, pp. 381–386, 2007

[4] N. Spruston, “Pyramidal neurons: dendritic structure and synaptic integration,” *Nat. Rev. Neurosci.*, vol. 9, no. 3, pp. 206–221, 2008

[5] E. R. Kandel, Y. Dudai, and M. R. Mayford, “The Molecular and Systems Biology of Memory,” *Cell*, vol. 157, no. 1, pp. 163–186, 2014

[6] R. Yuste, *Dendritic spines*. Cambridge, MA: MIT Press, 2010.

[7] J. C. Fiala, J. Spacek, and K. M. Harris, “Dendritic Spine Pathology: Cause or Consequence of Neurological Disorders?,” *Brain Res. Rev.*, vol. 39, no. 1, pp. 29–54, 2002

[8] W. Yu and B. Lu, “Synapses and Dendritic Spines as Pathogenic Targets in Alzheimer’s Disease,” *Neural Plast.*, vol. 2012, pp. 1–8, 2012

[9] P. Merino-Serrais *et al.*, “The influence of phospho-tau on dendritic spines of cortical pyramidal neurons in patients with Alzheimer’s disease,” *Brain*, vol. 136, no. 6, pp. 1913–1928, 2013

[10] J. Son et al., “Morphological change tracking of dendritic spines based on structural features,” *J. Microsc.*, vol. 241, no. 3, pp. 261–272, 2011

[11] E. Erdil et al., “Combining Nonparametric Spatial Context Priors With Nonparametric Shape Priors for Dendritic Spine Segmentation in 2-Photon Microscopy Images,” in *2019 IEEE 16th International Symposium on Biomedical Imaging (ISBI 2019)*, 2019, pp. 204–207.

[12] I. Vidaurre-Gallart *et al.*, “A Deep Learning-Based Workflow for Dendritic Spine Segmentation,” *Front. Neuroanat.*, vol. 16, 2022

[13] I. Y. Y. Koh et al., “An Image Analysis Algorithm for Dendritic Spines,” *Neural Comput.*, vol. 14, no. 6, pp. 1283–1310, 2002

[14] C. M. Weaver, P. R. Hof, S. L. Wearne, and W. B. Lindquist, “Automated Algorithms for Multiscale Morphometry of Neuronal Dendrites,” *Neural Comput.*, vol. 16, no. 7, pp. 1353–1383, 2004

[15] J. Cheng *et al.*, “A novel computational approach for automatic dendrite spines detection in two-photon laser scan microscopy,” *J. Neurosci. Methods*, vol. 165, no. 1, pp. 122–134, 2007

[16] A. Rodriguez, D. B. Ehlenberger, D. L. Dickstein, P. R. Hof, and S. L. Wearne, “Automated Three-Dimensional Detection and Shape Classification of Dendritic Spines from Fluorescence Microscopy Images,” *PLoS One*, vol. 3, no. 4, p. e1997, 2008

[17] S. Jain, S. Mukherjee, L. Danglot, and J.-C. Olivo-Marin, “Morphological Reconstruction of Detached Dendritic Spines via Geodesic Path Prediction,” in *2021 IEEE 18th International Symposium on Biomedical Imaging (ISBI)*, 2021, pp. 944–947.

[18] R. Su, C. Sun, C. Zhang, and T. D. Pham, “A novel method for dendritic spines detection based on directional morphological filter and shortest path,” *Comput. Med. Imaging Graph.*, vol. 38, no. 8, pp. 793–802, 2014

[19] A. F. Frangi, W. J. Niessen, K. L. Vincken, and M. A. Viergever, “Multiscale vessel enhancement filtering,” 1998, pp. 130–137.

[20] R. Benavides-Piccione et al., “Age-Based Comparison of Human Dendritic Spine Structure Using Complete Three-Dimensional Reconstructions,” *Cereb. Cortex*, vol. 23, no. 8, pp. 1798–1810, 2013

[21] F. de Chaumont *et al.*, “Icy: an open bioimage informatics platform for extended reproducible research,” *Nat. Methods*, vol. 9, no. 7, pp. 690–696, 2012

[22] N. Otsu, “A Threshold Selection Method from Gray-Level Histograms,” *IEEE Trans. Syst. Man. Cybern.*, vol. 9, no. 1, pp. 62–66, 1979

[23] C. Magliaro, A. L. Callara, N. Vanello, and A. Ahluwalia, “Gotta Trace ‘em All: A Mini-Review on Tools and Procedures for Segmenting Single Neurons Toward Deciphering the Structural Connectome,” *Front. Bioeng. Biotechnol.*, vol. 7, 2019

[24] E. Pchitskaya and I. Bezprozvanny, “Dendritic Spines Shape Analysis—Classification or Clusterization? Perspective,” *Front. Synaptic Neurosci.*, vol. 12, 2020

[25] F. Nourbakhsh *et al.*, “Neural Cell Segmentation in Large-Scale 3D Color Fluorescence Microscopy Images for Developemental Neuroscience,” in *2018 25th IEEE International Conference on Image Processing (ICIP)*, 2018, pp. 3828–3832.

[26] G. Mazzamuto et al., “Automatic Segmentation of Neurons in 3D Samples of Human Brain Cortex,” 2018, pp. 78–85.

[27] S. Basu, B. Condron, A. Aksel, and S. T. Acton, “Segmentation and Tracing of Single Neurons from 3D Confocal Microscope Images,” *IEEE J. Biomed. Heal. Informatics*, vol. 17, no. 2, pp. 319–335, 2013

[28] S. Mukherjee, B. Condron, and S. T. Acton, “Tubularity Flow Field—A Technique for Automatic Neuron Segmentation,” *IEEE Trans. Image Process.*, vol. 24, no. 1, pp. 374–389, 2015

[29] A. L. Callara, C. Magliaro, A. Ahluwalia, and N. Vanello, “A Smart Region-Growing Algorithm for Single-Neuron Segmentation From Confocal and 2-Photon Datasets,” *Front. Neuroinform.*, vol. 14, 2020

[30] T. Lindeberg, “Edge detection and ridge detection with automatic scale selection,” in *Proceedings CVPR IEEE Computer Society Conference on Computer Vision and Pattern Recognition*, 1996, pp. 465–470.